ACS APPLIED MATERIALS & INTERFACES

Research Article

www.acsami.org

Self-Powered Ultrafast Broadband Photodetector Based on p–n Heterojunctions of CuO/Si Nanowire Array

Qingshui Hong,[†,‡,§] Yang Cao,[†,§] Jia Xu,[⊥] Huimin Lu,[‡] Junhui He,*[,†] and Jia-Lin Sun*[,∥,#]

[†]Functional Nanomaterials Laboratory, Center for Micro/Nanomaterials and Technology and Key Laboratory of Photochemical Conversion and Optoelectronic Materials, Technical Institute of Physics and Chemistry, Chinese Academy of Sciences (CAS), Beijing 100190, China

[‡]School of Materials Science & Engineering, Beihang University, Beijing 100191, China

[⊥]Beijing Key Laboratory of Novel Thin Film Solar Cells, Renewable Energy School, North China Electric Power University, Beijing 102206, China

[∥]State Key Laboratory of Low-Dimensional Quantum Physics, Department of Physics, Tsinghua University, Beijing 100084, China

[#]Collaborative Innovation Center of Quantum Matter, Beijing, China

ABSTRACT: A new self-powered broadband photodetector was fabricated by coating an n-silicon nanowire (n-Si NW) array with a layer of p-cupric oxide (CuO) nanoflakes through a new simple solution synthesis method. The p–n heterojunction shows excellent rectification characteristics in the dark and distinctive photovoltaic behavior under broadband light illumination. The photoresponse of the detector at zero bias voltage shows that this self-powered photodetector is highly sensitive to visible and near-infrared light illuminations, with excellent stability and reproducibility. Ultrafast response rise and recovery times of 60 and 80 μs, respectively, are shown by the CuO based nanophotodetector. In addition, the broadband photodetector can also provide a rapid binary response, with current changing from positive to negative upon illumination under a small bias. The binary response arises from the photovoltaic behavior and the low turn-on voltage of the CuO/Si NW device. These properties make the CuO/Si NW broadband photodetector suitable for applications that require high response speeds and self-sufficient functionality.

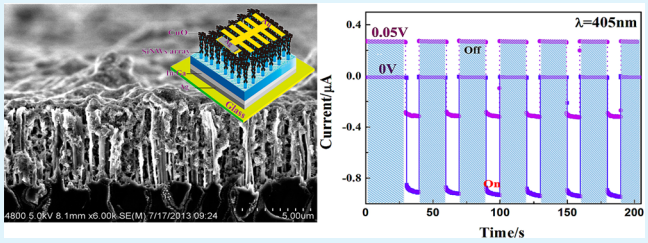

KEYWORDS: *self-powered, broadband photodetector, heterojunctions, silicon nanowire array, cupric oxide, response speed*

INTRODUCTION

Broadband photodetectors for the visible-infrared zone have a wide range of potential applications, including environmental and biological research, chemical analysis, imaging, and communications.[1−4] One-dimensional (1D) nanostructures, such as nanowires, nanoribbons and nanotubes, are promising candidate structures for the fabrication of high-performance photodetectors.[5] They generally offer the advantages of high sensitivity, low energy consumption, and high response speed because their low reflectance and high surface-to-volume ratio lead to increased photon collection efficiency and the low dimensions of the effective conductive channel shorten the transit times of the carriers. Various types of high-performance 1D nanostructure-based photodetectors have been reported, including devices based on ZnO, TiO_2, ZnS, CdS, CdSe, and CuO.[6−19] However, most of these devices operate with an external bias as the driving force, which greatly limits their independence in applications. In addition, their response speeds tend to be reduced because the external power sources cause local perturbations of the device depletion regions.[20] In recent years, it has been generally expected that functional nanosystems (where multiple nanoscale devices are integrated) must be fully functional, and must not only have sensing, communication, control, and actuation/response capabilities, but must also be self-sufficient. For example, a self-driven nanoscale photodetector that is easy to use and has high sensitivity, high response speed, and low cost is highly desirable for biochemical analysis and air-pollution monitoring systems. Recently, several reports on these self-powered photodetectors with high response speeds have demonstrated the possibility that these photodetectors can function independently of external power sources. These photodetectors can work under nominal zero-volt position or short-circuit conditions based on the photovoltaic behavior characteristics of these devices, which were driven by Schottky junctions or p-n heterojunctions without the need to consume external power, but the range of detectable light wavelengths is generally very narrow and the limitations of the detectable light intensity are always high (UV region, ca. 200 W cm^{-2} level).[16,21−24] It is therefore still a significant challenge to fabricate simple nanoscale devices toward self-powered broadband detectors with high photosensitivity and high response speeds under

Received: August 14, 2014
Accepted: November 10, 2014
Published: November 10, 2014

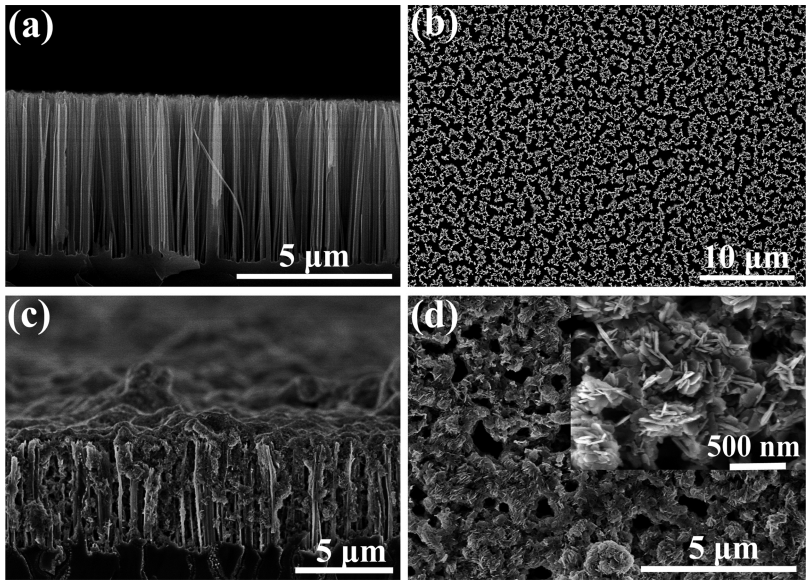

Figure 1. (a) Cross-sectional view and (b) top view SEM images of a Si NW array. (c) Cross-sectional and (d) large area and (inset) magnified surface SEM images of the CuO/Si NW heterojunction formed via a solution synthesis method with 20 deposition cycles.

weak light conditions, which will be very promising for applications in future nano-optoelectronic integrated circuits.

Nanostructured transition metal oxides, which have been an indisputable prerequisite for the development of various novel functional and smart materials, have attracted considerable attention from researchers because of their unique physical and chemical properties.[25] CuO is an increasingly well-studied transition metal oxide for optoelectronic device applications because of its interesting properties as a p-type semiconductor with a narrow band gap (1.35 eV), along with its high theoretical capacity, safety, environmental friendliness, chemical durability, and radiation resistance.[26,27] In this paper, we use a p-type nanoscale CuO layer and an n-type vertically aligned array of Si NWs to form a 1D p-n heterostructure. We show that the device performs as a self-powered broadband detector that responds to visible and near-infrared light at zero bias with high photosensitivity (1×10^3), which was defined as $(I_{light} - I_{dark})/I_{dark}$, for low intensity irradiance (0.48 W cm^{-2}). The CuO/Si NW array photodetector exhibited an ultrafast photoresponse with 60 μs rise time and 80 μs recovery time. In addition, the photodetector, when working under a small forward bias, showed a binary response to broadband light with high speed.

EXPERIMENTAL SECTION

Device Fabrication. Arrays of vertical silicon nanowires were fabricated from a commercial Si wafer [n-type, (111)-oriented, 0.01 Ω•cm] by an Ag-assisted electroless etching method. A small piece of the Si wafer (1.2 × 1.2 cm^2 in size) was etched in 0.15 M H_2O_2 for 40 min following the method of Cao et al.[28] Subsequently, the CuO layer was deposited on the Si NWs without using any surfactants. The typical deposition process was as follows: first, a drop of NaOH (20 μL, 0.1 M in ethanol), a drop of $Cu(NO_3)_2$ (20 μL, 0.1 M in ethanol) and a drop of $NH_3 \cdot H_2O$ (20 μL, 5 M) were dripped on the surfaces of the Si NWs. Then, the sample was placed in a preheated oven at 80 °C for 5 min. This synthesis process was repeated 20 times to increase the amount of CuO that was deposited. Finally, the sample was rinsed several times with deionized water to remove any extra ions and dried under a N_2 flow. A patterned gold contact was then deposited to create the top electrode. The bottom ohmic contact was formed by coating eutectic In:Ga on the reverse of the n-Si substrate.[29]

Structural Characterization and Testing of Photoelectric Properties. The morphologies of the Si NWs before and after deposition of CuO were characterized using a Hitachi S4800 field-emission SEM (FESEM). For TEM observations, the arrays of Si NWs that were coated with CuO were dispersed in ethanol by sonication for 10 min, and then added to carbon-coated copper grids. After drying overnight at 60 °C, the structures were observed on a JEOL JEM-2100F TEM. A Bruker-D8 X-ray diffractometer with Cu−Kα radiation (0.154056 nm) was used to evaluate the crystalline properties of the sample. A Keithley 2400 (set to apply 0.00 V) was used to characterize the electrical properties of the CuO/Si NW device. All measurements were carried out at room temperature under ambient conditions. Three lasers with wavelengths of 405, 532, and 1064 nm were used as light sources. The high speed features of the device were measured using a chopper and a precision source/measurement unit (Agilent B2911A).

RESULTS AND DISCUSSION

Structural and Morphological Characterization. An array of Si NWs was fabricated by a previously reported method.[28] Figure 1a, b shows the cross-sectional view and top view scanning electron microscopy (SEM) images of the as-fabricated Si NW array, respectively. From the cross-sectional view shown in Figure 1a, the high density Si NWs are easily distinguishable, uniform and vertical to the Si wafer substrate. The average length of the Si NWs is about 5 μm and the diameters ranged from 50 to 400 nm. The top view of Figure 1b with low magnification also indicates that the Si NWs are formed with high density and highly ordered over a large area.

To fabricate the p-CuO/n-Si NW heterojunction, we deposited a CuO layer on the Si NWs, with the synthesis process repeated 20 times. Cross-sectional and surface SEM images of the sample after deposition of the CuO layer are shown in images c and d in Figure 1, respectively. Figure 1c clearly shows that each Si NW was wrapped by a large number of CuO nanoflakes, forming a pseudo core−shell structure that could provide a high surface area for the p−n interface. It is noted that the Si NWs retained their array morphology without significant reduction in length. This indicates that the CuO/Si NW heterojunction preparation process had not caused significant corrosion to the original Si NWs. The surface

SEM image (Figure 1d) shows that the highly dense CuO nanoflakes were deposited on top of each Si NW. It should be noted that the most of the spaces between the Si NWs were not filled by the CuO nanoflakes, which was conducive to high-efficiency light harvesting. The inset of Figure 1d shows that the CuO layer consisted of numerous flake-like nanostructures with thicknesses of ~20 nm. Without the need for any annealing process or postprocess treatments, a CuO layer formed with excellent adhesion on the surfaces of the Si NWs, and this layer could endure repeated washing with deionized water.

Figure 2a compares the X-ray diffraction (XRD) patterns of the Si NW array and the CuO-coated Si NW array. Figure 2a

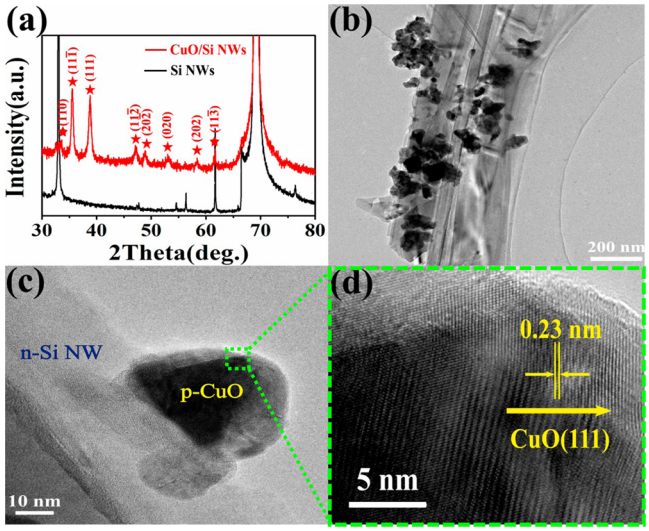

Figure 2. (a) XRD patterns of the CuO/Si NW array and the Si NW array. (b) TEM image of the CuO/Si NW structure at low magnification. (c) Medium magnification and (d) high-resolution TEM (HRTEM) images of an individual CuO flake coated on a single Si NW.

clearly shows that CuO was successfully grown on the surface of the Si NWs. In detail, the peak positions of the CuO/Si NW array (red line) exhibited the monoclinic structure of CuO, which was confirmed by the International Center for Diffraction Data (ICDD) card No. 45−0937. The mean crystalline size of CuO was calculated to be ca. 25 nm using the Scherrer formula. In addition, no other impurity peaks were detected in the XRD pattern, indicating the formation of a single CuO phase. Figure 2b is a low-magnification transmission electron microscopy (TEM) image of the as-prepared CuO/Si NWs. The image shows that CuO was deposited on the surface of the Si NWs. Images c and d in Figure 2 are medium-magnification TEM and high-resolution TEM (HRTEM) images, respectively, of an individual CuO flake coated on a single Si NW. The HRTEM image (Figure 2d) shows that the CuO on the edge of the Si NW had a lattice plane distance of 0.23 nm, which corresponds to the (111) plane distance of monoclinic CuO.

Properties of the Self-Powered Photodetector Based on the CuO/Si NW p-n Heterojunction Array. Figure 3a shows a schematic diagram and a digital photograph of the p-CuO/n-Si NW photodetector. Figure 3b shows a typical current−voltage (I−V) curve under dark conditions, and the corresponding semilog I−V plot is also given as inset. The results clearly exhibit a rectifying characteristic and also

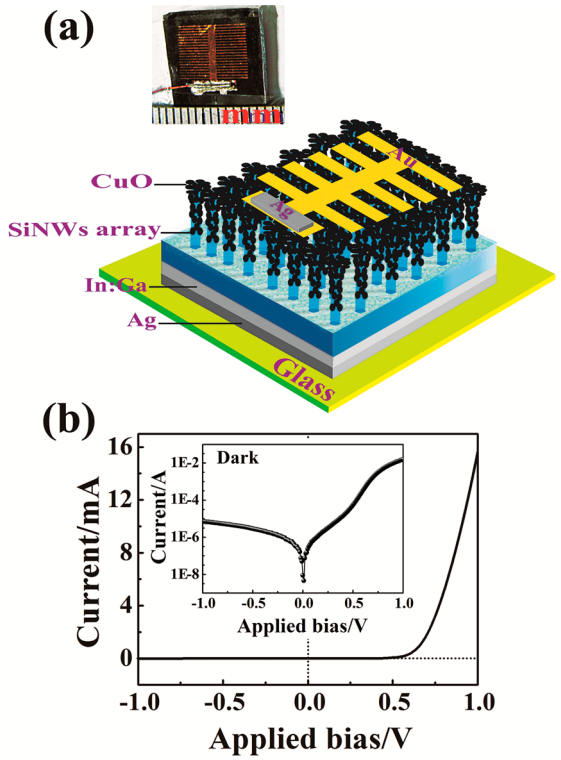

Figure 3. (a) Schematic diagram of the p-CuO/n-Si NW array photodetector, the inset shows a digital photograph of the device. (b) Linear and semilogarithmic (inset) plots of current and voltage for the device in the dark, respectively.

demonstrate that the CuO/Si NW heterojunctions behaved as well-defined diodes with a rectification ratio of 1600 at bias voltages of −1 and 1 V. The turn-on voltage was approximately 0.7 V. This rectification behavior must mainly arise from the CuO/Si NW contact, if we consider the fact that the contact between Au and CuO and that between In:Ga and Si were both ohmic-type contacts.[30,31]

The I−V characteristics under visible and near-infrared illuminations were investigated using 405 nm (0.48 W cm^{-2}, spot size of 2.5 mm^2), 532 nm (5 W cm^{-2}, spot size of 4 mm^2) and 1064 nm (5.5 W cm^{-2}, spot size of 6.2 mm^2) lasers as illumination sources. Figure 4a−c show the I−V curves of the heterojunction under illumination by these three light sources, with the dark characteristics shown for comparison in each case. Two significant features were observed in all the I−V curves: first, a small but measurable photovoltaic effect was observed under the three different illuminations; second, under a small forward bias, the photodetector current changed from positive to negative (i.e., a binary current phenomenon) in response to the light sources being switched off and on.

Figure 4d−f shows the photoresponses of the device under zero bias and under a small forward bias for each of the three illumination sources. Six cycles of switching the laser on and off demonstrated the good stability and reproducibility of the photoresponse. The steep rise and fall edges indicated the fast response of the device. In addition, the photosensitivity of the photodetector was obtained from the photoresponse under zero bias. The photosensitivities under zero bias were 1371, 6289, and 7028 for the wavelengths of 405, 532, and 1064 nm, respectively. The much lower illumination intensity of 405 nm laser led to the lower photosensitivity at 405 nm than at 532 and 1064 nm. These values were high and rank among the best

dx.doi.org/10.1021/am5054338 | ACS Appl. Mater. Interfaces 2014, 6, 20887−20894

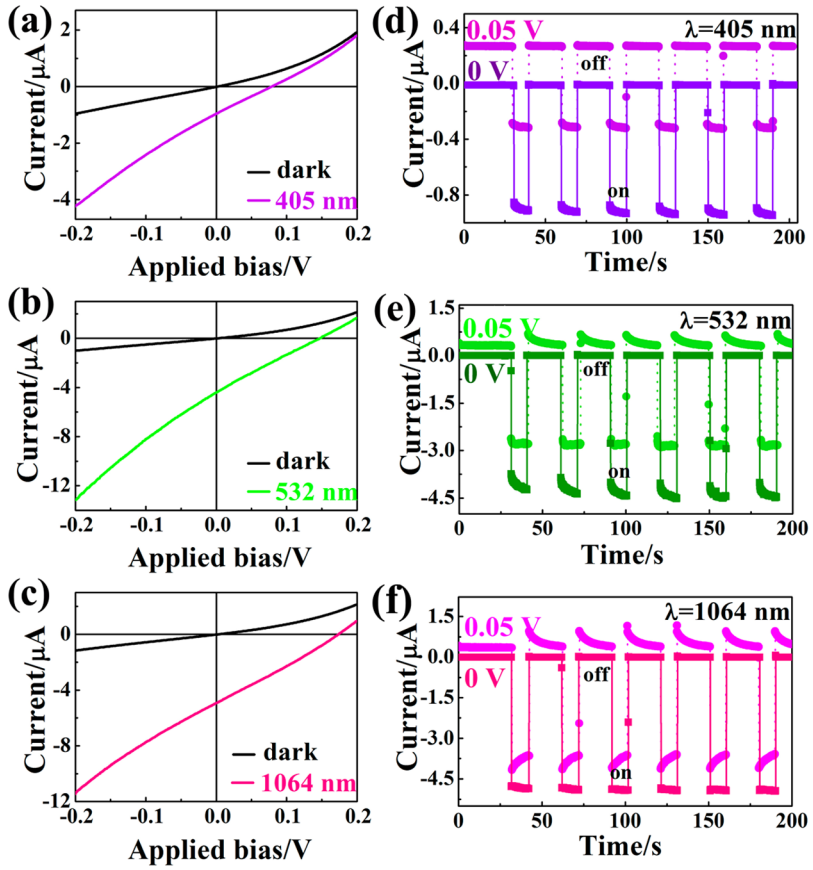

Figure 4. Photoelectric properties of the CuO/Si NW array photodetector under illumination at various wavelengths. (a–c) *I*–*V* characteristics. (d–f) Photoresponses under zero bias and under a small forward bias when irradiation is turned on (10 s) and off (20 s), repeated for six cycles. The light wavelengths are (a, d) 405, (b, e) 532, and (c, f) 1064 nm.

values reported to date for p–n heterojunction-based photodetectors. The high photosensitivity of the device is attributed to the combined actions of the Si NW array and the CuO layer. The aligned Si NW array structure can greatly suppress light reflection over a wide spectral range, from visible to near-infrared.[32] This could significantly improve the light harvesting of the device and result in the high photocurrent. Meanwhile, the built-in electric field within the p-CuO/n-Si NW array junction could also guarantee both a high photocurrent and a low dark current (0.7 nA at zero bias).

Moreover, under a small forward bias, the current was observed to alternate between positive and negative when the three light sources were switched off and on. These changes in the currents were matched by the *I*–*V* characteristics of the device shown in Figure 4a–c, which could explain the origin of the binary response under the small forward bias. In the dark, the small forward bias could produce a positive current in the circuit, while upon illumination, the photoinduced electromotive force was in the reverse direction to the applied bias, and therefore led to the current change from positive to negative. And the relatively significant variation of dark currents when 532 nm (5 W cm^{-2}) and 1064 nm (5.5 W cm^{-2}) lasers were turned off may arise from the thermal effect of radiations caused by relatively high-power density irradiation. This phenomenon offers the opportunity to use the device as an on–off binary response device for broadband photodetection that can exceed the highest previously recorded photosensitivities of ~1 × 10^5.[16,33]

The photoresponse of the CuO/Si NW array device was tested under various irradiance intensities for the three light sources. Figure 5a–c show steadily increasing photocurrent responses with increasing irradiance intensity for all three light sources, producing photocurrents of 0.96 μA at 0.48 W cm^{-2} for the 405 nm laser, 4.41 μA at 5 W cm^{-2} for the 532 nm laser and 4.92 μA at 5.5 W cm^{-2} for the 1064 nm laser. This dependence of photocurrent on irradiance intensity can be fitted by a simple power law: $I = AP^{\theta}$, where I is the photocurrent, A is a constant at a specific wavelength, P is the power density of the incident light, and θ is a parameter related to the trapping and recombination processes of the photocarriers in photodetectors.[34,35] Fitting of these curves showed that θ = 0.63, 0.64, and 0.66 for the wavelengths of 405, 532, and 1064 nm (see Figure 5d–f), respectively. This fractional power dependence is likely to be related to the carrier traps on the CuO surface.[35]

To evaluate the detection performance of the CuO/Si NW photodetector, the responsivity (R), detectivity (D^*) and photoconductive gain (G) of the photodetector were determined. R is defined as the photocurrent generated per unit of incident power. D^* is normalized to the active detector area (A) and the equivalent noise bandwidth, and is commonly used as a material figure of merit to describe the photoconductor sensitivity. G is defined as the number of carriers produced in the external circuit for each absorbed incident photon. These three parameters can be expressed using the following equations

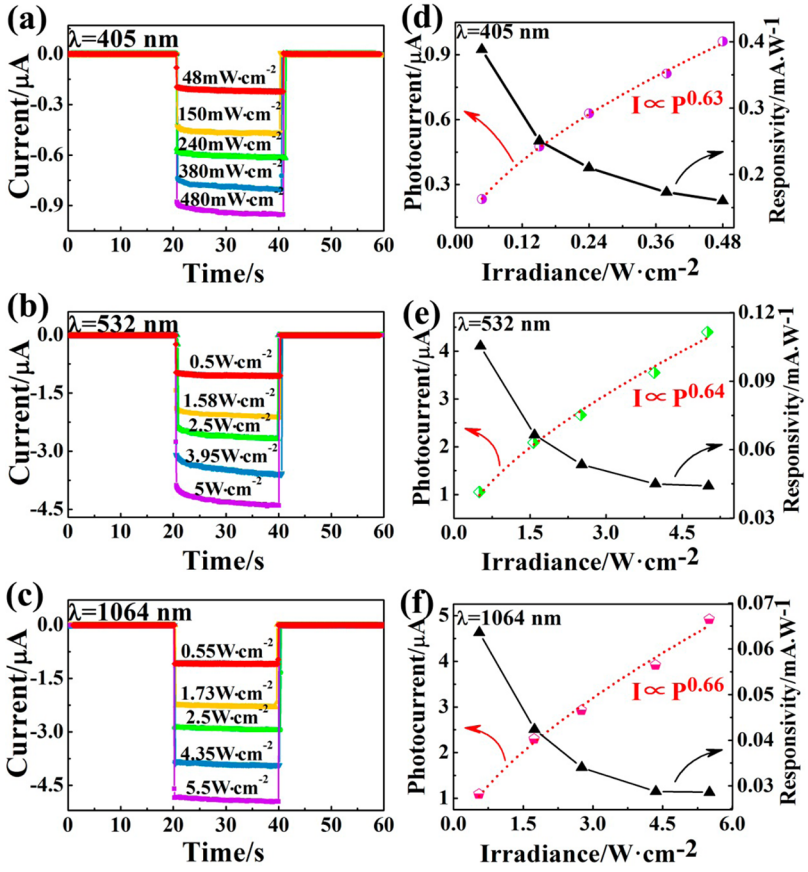

Figure 5. (a–c) Photoresponses under zero bias to illumination at various intensities from the 405, 532, and 1064 nm lasers. (d–f) Left: fitting curves for the relationships between the photocurrent and the light intensity for the 405, 532, and 1064 nm lasers; Right: device responsivity to the various intensities of the 405, 532, and 1064 nm lasers.

$$R(\mathrm{AW}^{-1}) = \frac{\Delta I}{AP}$$

$$D^* = \frac{A^{1/2}R}{(2eI_{\mathrm{dark}})^{1/2}}$$

$$G = \left[\frac{\Delta I}{AP\eta}\right]\left(\frac{h\nu}{\mathrm{e}}\right)$$

Where ΔI is the photocurrent, which is defined as the difference between the current in the dark and under illumination, A is the active contact area (half of the light spot area, when taking the electrode configuration into consideration), P is the laser power density, η is the effective photocarrier generation efficiency (which is assumed to be 0.7 in our work, when taking the scattering, reflection, and incomplete absorption into consideration), h is Planck's constant, ν is the frequency of the incident light, e is the electron charge, and I_{dark} is the dark current. In all cases (Figure 5d–f), the responsivity was shown to decrease, although not significantly, with increasing illumination intensity. The results for all parameters are summarized in Table 1. It is noted that the device has low responsivity and detectivity, which is common for self-powered detectors that always have low responsivity and detectivity (ca. mA W^{-1} or 1×10^9 cm $Hz^{1/2}$ W^{-1}) because there is not an external electric field to drive the excitons dissociation. However, the excitons separation solely by the built-in electric field would still be able to guarantee the self-powered device to detect light irradiation. Furthermore, it can be seen that the R, D^*, and G values are obviously greater under illumination by the 405 and 532 nm lasers than under the 1064 nm illumination. This can be explained as follows: when the CuO/Si NW array heterojunction was irradiated by the 405 or 532 nm lasers, photoexcitation occurred in both CuO and the Si NW array because the photoenergies of the 405 nm beam (~3.06 eV) and the 532 nm beam (~2.33 eV) are higher than the bandgaps of both CuO (~1.35 eV) and Si (~1.12 eV). In contrast, when the CuO/Si NW array heterojunction was irradiated by the 1064 nm laser, photoexcitation only occurred in the Si NWs, because the photoenergy of the 1064 nm beam (~1.17 eV) is lower than the bandgap of CuO.

Table 1. Typical Photoelectric Properties of the CuO/Si NW Photodetector

wavelength (nm)	P (W cm^{-2})	R (mA W^{-1})	D^* (cm $Hz^{1/2}$ W^{-1})	G
405	0.0480	0.389	3.00×10^9	0.00169
532	0.500	0.105	1.00×10^9	0.000350
1064	0.550	0.064	7.60×10^8	0.000110

The photocurrent rise and recovery times were measured using a mechanical light chopper, a 532 nm laser and a precision source/measurement unit (Agilent B2911A), as seen in Figure 6a. The test was conducted under a nominal zero applied field. Figure 6b shows the photocurrent responses of the self-powered photodetector under light switching frequen-

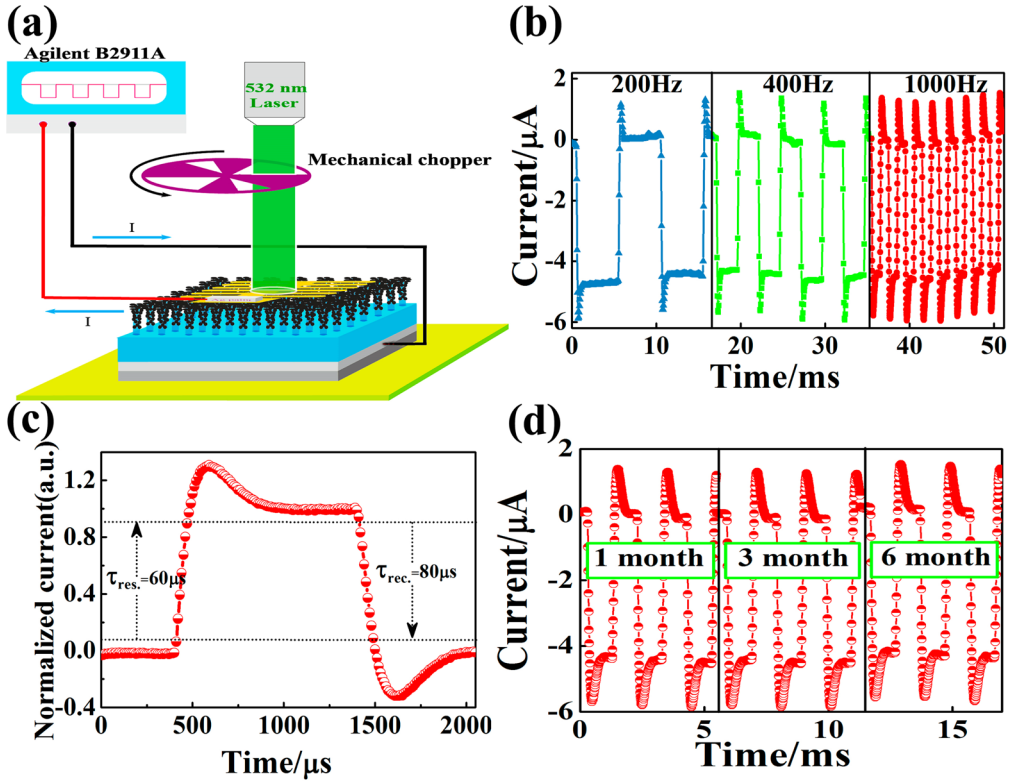

Figure 6. (a) Schematic illustration of the measurement configuration for photoresponse speed measurement. (b) Photocurrent response of the photodetector at light switching frequencies of 200, 400, and 1000 Hz. (c) Single normalized modulation cycle measured at 1000 Hz. (d) Photoresponse behavior of the photodetector under atmospheric conditions for more than 6 months.

cies of 200, 400, and 1000 Hz. For all switching frequencies, the response was fast and showed good stability and repeatability. This result suggests that the CuO/SiNW heterojunction photodetector can work well over a wide switching frequency range, which is vitally important to monitor the ultrafast optical signal. In the time domain, photodetector response speed is normally assessed based on the response time (τ_{res}), which is defined as the time interval required for the response to rise from 10% to 90% of its peak value, and the recovery time (τ_{rec}) is defined analogously. Figure 6c shows a single normalized modulation cycle measured at 1000 Hz. The time interval between two collected data points was 10 μs when the current−time profile was recorded using the precision source/measurement unit (Agilent B2911A). The response time and the recovery time were thus found to be approximately 60 and 80 μs, respectively. These values were among the best reported, to our knowledge, for self-powered photodetectors[16−18,23,36] and at least 10^5 times faster than those previously reported for CuO based photodetectors (Table 2).[15,26,30,37] In addition, according to a previous report, a chopped laser would introduce extra response and recovery times of about 35 and 32 μs for this level of switching frequency, respectively.[36] Thus, we believed that the real response and recovery times of the current device should actually be shorter. The relatively high response speed is attributed to the extremely high carrier mobility and the rapid separation of huge numbers of photogenerated carriers under the built-in electric field formed at the CuO/Si NW interface. It should also be noted that this CuO/Si NW device did not require the surface to be specially treated with absorbing polymers or to be encapsulated to prevent degradation. The devices were stable under atmospheric conditions for more than six months with no sign of reduced photodetection performance (see Figure 6d).

Table 2. Comparison of the Response Speed of the CuO/Si NW Photodetector and Other CuO-Based Photodetectors

photodetector	response time	recover time	ref
p-CuO/n-Si NW array	60 μs	80 μs	this work
p-CuO/n-ZnO NW	1.3 s	1.2 s	26
Ag/CuO NW	40 s	36 s	15
ZnO/CuO NW array	4.2 s	5.2 s	30
Ag/CuO NW	15 s	17 s	37

Finally, we investigated the photovoltaic characteristics of the self-powered CuO/Si NW photodetector from the perspective of the energy band diagram shown in Figure 7, which was proposed according to the Anderson−Shockley model. E_F is the Fermi level, E_{g1} is the bandgap of n-SiNW, and E_{g2} is the bandgap of CuO. When the CuO layer was deposited on the Si NWs, a depletion region formed on both the Si and CuO sides by carrier diffusion under thermal equilibrium conditions, leading to the formation of a built-in electric field near the CuO/Si NW interface. Under above-bandgap light illumination, the photogenerated holes (h) and electrons (e) within the depletion region would be readily driven toward p-CuO and n-Si NW, respectively, by the built-in electric field, leading to generation of a photovoltaic current in the external circuit. In addition, the minority carriers generated within the diffusion length from the depletion region could also diffuse to the depletion region and be extracted by the built-in electric field. The photovoltage was a result of the energy difference between the Fermi levels of CuO and Si NWs under illumination. This photovoltaic effect enabled the current device to sense visible

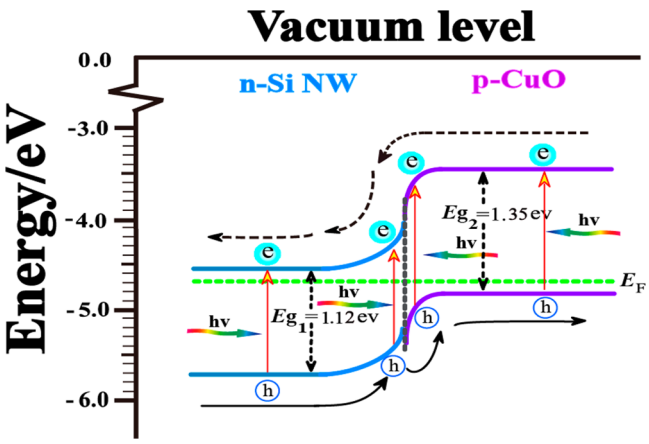

Figure 7. Energy-band diagram of the p-CuO/n-Si NW array photodetector showing the photogenerated carrier transfer process under illumination and at zero bias.

and near-infrared illumination without any external energy supply.

CONCLUSIONS

In summary, we have fabricated and studied a self-powered CuO/Si NW-based broadband photodetector for the first time. Under relatively weak visible and near-infrared light illumination, the device showed high photosensitivity and ultrafast response speeds under zero bias, and revealed a distinctive binary response under a small forward bias. These merits are attributed to the advantages of the geometry of the arrayed nanowires, the high surface area, and the built-in field near the CuO/Si NW interface. This broadband photodetector, with its features of easy fabrication, high photosensitivity, self-sufficiency, and good stability, has huge application potential in the fields of environmental sensing, biosensing, binary switching, and optoelectronic integrated circuits.

AUTHOR INFORMATION

Corresponding Authors

*E-mail: jhhe@mail.ipc.ac.cn.

*E-mail: jlsun@tsinghua.edu.cn.

Author Contributions

[§]Q.H. and Y.C. contributed equally to this work.

Notes

The authors declare no competing financial interest.

ACKNOWLEDGMENTS

This work was supported by the National Natural Science Foundation of China (Grants 11104283, 21271177, 11174172, and 51302081), Technical Institute of Physics and Chemistry, Chinese Academy of Sciences, the National Basic Research Program of China (Grant 2010CB934103), and the Open Research Fund Program of the State Key Laboratory of Low-Dimensional Quantum Physics (Grant KF201207).

REFERENCES

(1) Hu, L.; Zhu, L.; He, H.; Guo, Y.; Pan, G.; Jiang, J.; Jin, Y.; Sun, L.; Ye, Z. Colloidal Chemically Fabricated ZnO: Cu-based Photodetector with Extended UV-visible Detection Waveband. *Nanoscale* **2013**, *5*, 9577−9581.

(2) Zou, Z.; Xie, C.; Zhang, S.; Yang, C.; Zhang, G.; Yang, L. CdS/ZnO Nanocomposite Film and its Enhanced Photoelectric Response to UV and Visible Lights at Low Bias. *Sens. Actuators, B* **2013**, *188*, 1158−1166.

(3) Chen, G.; Liang, B.; Liu, X.; Liu, Z.; Yu, G.; Xie, X.; Luo, T.; Chen, D.; Zhu, M.; Shen, G.; Fan, Z. High-Performance Hybrid Phenyl-C61-Butyric Acid Methyl Ester/Cd3P2 Nanowire Ultraviolet−Visible−Near Infrared Photodetectors. *ACS Nano* **2013**, *8*, 787−796.

(4) Zhan, Z.; Zheng, L.; Pan, Y.; Sun, G.; Li, L. Self-powered, Visible-light Photodetector Based on Thermally Reduced Graphene Oxide-ZnO (rGO-ZnO) Hybrid Nanostructure. *J. Mater. Chem.* **2012**, *22*, 2589−2595.

(5) Zhai, T.; Li, L.; Wang, X.; Fang, X.; Bando, Y.; Golberg, D. Recent Developments in One-Dimensional Inorganic Nanostructures for Photodetectors. *Adv. Funct. Mater.* **2010**, *20*, 4233−4248.

(6) Lin, P.; Yan, X.; Zhang, Z.; Shen, Y.; Zhao, Y.; Bai, Z.; Zhang, Y. Self-Powered UV Photosensor Based on PEDOT:PSS/ZnO Micro/Nanowire with Strain-Modulated Photoresponse. *ACS Appl. Mater. Interfaces* **2013**, *5*, 3671−3676.

(7) Mahmood, K.; Swain, B. S.; Han, G.-S.; Kim, B.-J.; Jung, H. S. Polyethylenimine-Assisted Growth of High-Aspect-Ratio Nitrogen-Doped ZnO (NZO) Nanorod Arrays and Their Effect on Performance of Dye-Sensitized Solar Cells. *ACS Appl. Mater. Interfaces* **2014**, *6*, 10028−10043.

(8) Shinde, S. S.; Rajpure, K. Y. Fabrication and performance of N-doped ZnO UV photoconductive detector. *J. Alloys Compd.* **2012**, *522*, 118−122.

(9) Shinde, S. S.; Bhosale, C. H.; Rajpure, K. Y. N-doped ZnO based fast response ultraviolet photoconductive detector. *Solid-State Electron.* **2012**, *68*, 22−26.

(10) Game, O.; Singh, U.; Kumari, T.; Banpurkar, A.; Ogale, S. ZnO(N)-Spiro-MeOTAD hybrid photodiode: an efficient self-powered fast-response UV (visible) photosensor. *Nanoscale* **2014**, *6*, 503−513.

(11) Ye, Y.; Dai, L.; Wen, X.; Wu, P.; Pen, R.; Qin, G. High-Performance Single CdS Nanobelt Metal-Semiconductor Field-Effect Transistor-Based Photodetectors. *ACS Appl. Mater. Interfaces* **2010**, *2*, 2724−2727.

(12) Yang, Q.; Guo, X.; Wang, W.; Zhang, Y.; Xu, S.; Lien, D. H.; Wang, Z. L. Enhancing Sensitivity of a Single ZnO Micro-/Nanowire Photodetector by Piezo-phototronic Effect. *ACS Nano* **2010**, *4*, 6285−6291.

(13) Zhang, F.; Ding, Y.; Zhang, Y.; Zhang, X.; Wang, Z. L. Piezo-phototronic Effect Enhanced Visible and Ultraviolet Photodetection Using a ZnO−CdS Core−Shell Micro/nanowire. *ACS Nano* **2012**, *6*, 9229−9236.

(14) Wei, T.-Y.; Huang, C.-T.; Hansen, B. J.; Lin, Y.-F.; Chen, L.-J.; Lu, S.-Y.; Wang, Z. L. Large Enhancement in Photon Detection Sensitivity via Schottky-gated CdS Nanowire Nanosensors. *Appl. Phys. Lett.* **2010**, *96*, 013508.

(15) Wang, S.-B.; Hsiao, C.-H.; Chang, S.-J.; Jiao, Z. Y.; Young, S.-J.; Hung, S.-C.; Huang, B.-R. ZnO Branched Nanowires and the p-CuO/n-ZnO Heterojunction Nanostructured Photodetector. *IEEE T. Nanotechnol* **2013**, *12*, 263−269.

(16) Jin, W.; Ye, Y.; Gan, L.; Yu, B.; Wu, P.; Dai, Y.; Meng, H.; Guo, X.; Dai, L. Self-powered High Performance Photodetectors Based on CdSe Nanobelt/graphene Schottky Junctions. *J. Mater. Chem.* **2012**, *22*, 2863−2867.

(17) Wu, D.; Jiang, Y.; Zhang, Y.; Yu, Y.; Zhu, Z.; Lan, X.; Li, F.; Wu, C.; Wang, L.; Luo, L. Self-powered and Fast-speed Photodetectors Based on CdS:Ga Nanoribbon/Au Schottky Diodes. *J. Mater. Chem.* **2012**, *22* (43), 23272−23276.

(18) Ni, P.-N.; Shan, C.-X.; Wang, S.-P.; Liu, X.-Y.; Shen, D.-Z. Self-powered Spectrum-selective Photodetectors Fabricated from n-ZnO/p-NiO Core-shell Nanowire Arrays. *J. Mater. Chem.C* **2013**, *1*, 4445−4449.

(19) Han, Y.; Fan, C.; Wu, G.; Chen, H.-Z.; Wang, M. Low-Temperature Solution Processed Utraviolet Photodetector Based on an Ordered TiO2 Nanorod Array−Polymer Hybrid. *J. Mater. Chem.C* **2011**, *115*, 13438−13445.

(20) Soci, C.; Zhang, A.; Xiang, B.; Dayeh, S. A.; Aplin, D. P. R.; Park, J.; Bao, X. Y.; Lo, Y. H.; Wang, D. ZnO Nanowire UV Photodetectors with High Internal Gain. *Nano Lett.* **2007**, *7*, 1003−1009.
(21) Yang, Q.; Liu, Y.; Li, Z.; Yang, Z.; Wang, X.; Wang, Z. L. Self-Powered Ultrasensitive Nanowire Photodetector Driven by a Hybridized Microbial Fuel Cell. *Angew. Chem., Int. Ed.* **2012**, *51*, 6443−6446.
(22) Zeng, L. H.; Wang, M. Z.; Hu, H.; Nie, B.; Yu, Y. Q.; Wu, C. Y.; Wang, L.; Hu, J. G.; Xie, C.; Liang, F. X.; Luo, L. B. Monolayer Graphene/Germanium Schottky Junction As High-Performance Self-Driven Infrared Light Photodetector. *ACS Appl. Mater. Interfaces* **2013**, *5*, 9362−9366.
(23) Bie, Y. Q.; Liao, Z. M.; Zhang, H. Z.; Li, G. R.; Ye, Y.; Zhou, Y. B.; Xu, J.; Qin, Z. X.; Dai, L.; Yu, D. P. Self-Powered, Ultrafast, Visible-Blind UV Detection and Optical Logical Operation based on ZnO/GaN Nanoscale p-n Junctions. *Adv. Mater.* **2011**, *23*, 649−653.
(24) Gao, C.; Li, X.; Wang, Y.; Chen, L.; Pan, X.; Zhang, Z.; Xie, E. Titanium Dioxide Coated Zinc Oxide Nanostrawberry Aggregates for Dye-sensitized Solar Cell and Self-powered UV-Photodetector. *J. Power Sources* **2013**, *239*, 458−465.
(25) Zhang, Q. B.; Zhang, K. L.; Xu, D. G.; Yang, G. C.; Huang, H.; Nie, F. D.; Liu, C. M.; Yang, S. H. CuO Nanostructures: Synthesis, Characterization, Growth Mechanisms, Fundamental Properties, and Applications. *Prog. Mater. Sci.* **2014**, *60*, 208−337.
(26) Hsueh, H. T.; Chang, S. J.; Weng, W. Y.; Hsu, C. L.; Hsueh, T. J.; Hung, F. Y.; Wu, S. L.; Dai, B. T. Fabrication and Characterization of Coaxial p-Copper Oxide/n-ZnO Nanowire Photodiodes. *Ieee. T. Nanotechnol.* **2012**, *11*, 127−133.
(27) Wu, J.-K.; Chen, W.-J.; Chang, Y. H.; Chen, Y. F.; Hang, D.-R.; Liang, C.-T.; Lu, J.-Y. Fabrication and Photoresponse of ZnO Nanowires/CuO Coaxial Heterojunction. *Nanoscale Res. Lett.* **2013**, *8*, 1−5.
(28) Cao, Y.; He, J.-H.; Zhu, J.-L.; Sun, J.-L. Fabrication of Carbon Nanotube/silicon Nanowire Array Heterojunctions and Their Silicon Nanowire Length Dependent Photoresponses. *Chem. Phys. Lett.* **2011**, *501*, 461−465.
(29) Shen, X.; Sun, B.; Liu, D.; Lee, S.-T. Hybrid Heterojunction Solar Cell Based on Organic−Inorganic Silicon Nanowire Array Architecture. *J. Am. Chem. Soc.* **2011**, *133*, 19408−19415.
(30) Tian, W.; Zhi, C.; Zhai, T.; Wang, X.; Liao, M.; Li, S.; Chen, S.; Golberg, D.; Bando, Y. Ultrahigh Quantum Efficiency of CuO Nanoparticle Decorated In2Ge2O7 Nanobelt Deep-ultraviolet Photodetectors. *Nanoscale* **2012**, *4*, 6318−6324.
(31) Wang, P.; Zhao, X.; Li, B. ZnO-coated CuO Nanowire Arrays: Fabrications, Optoelectronic Properties, and Photovoltaic Applications. *Opt. Express* **2011**, *19*, 11271−11279.
(32) Peng, K. Q.; Xu, Y.; Wu, Y.; Yan, Y. J.; Lee, S. T.; Zhu, J. Aligned Single-crystalline Si Nanowire Arrays for Photovoltaic Applications. *Small* **2005**, *1*, 1062−1067.
(33) Hatch, S. M.; Briscoe, J.; Dunn, S. A Self-Powered ZnO-Nanorod/CuSCN UV Photodetector Exhibiting Rapid Response. *Adv. Mater.* **2013**, *25*, 867−871.
(34) Kind, H.; Yan, H. Q.; Messer, B.; Law, M.; Yang, P. D. Nanowire Ultraviolet Photodetectors and Optical Switches. *Adv. Mater.* **2002**, *14*, 158−160.
(35) Wu, D.; Jiang, Y.; Zhang, Y. G.; Li, J. W.; Yu, Y. Q.; Zhang, Y. P.; Zhu, Z. F.; Wang, L.; Wu, C. Y.; Luo, L. B.; Jie, J. S. Device Structure-dependent Field-effect and Photoresponse Performances of p-type ZnTe:Sb Nanoribbons. *J. Mater. Chem.* **2012**, *22*, 6206−6212.
(36) Gao, Z.; Jin, W.; Zhou, Y.; Dai, Y.; Yu, B.; Liu, C.; Xu, W.; Li, Y.; Peng, H.; Liu, Z.; Dai, L. Self-powered Flexible and Transparent Photovoltaic Detectors Based on CdSe Nanobelt/graphene Schottky Junctions. *Nanoscale* **2013**, *5*, 5576−5581.
(37) Hansen, B. J.; Kouklin, N.; Lu, G.; Lin, I. K.; Chen, J.; Zhang, X. Transport, Analyte Detection, and Opto-Electronic Response of p-Type CuO Nanowires. *J. Phys. Chem. C* **2010**, *114*, 2440−2447.